Optical and compositional properties of amorphous silicon-germanium films by plasma processing for integrated photonics

William W. Hernández-Montero,[*] Ignacio E. Zaldívar-Huerta, Carlos Zúñiga-Islas, Alfonso Torres-Jácome, Claudia Reyes-Betanzo, and Adrián Itzmoyotl-Toxqui

Instituto Nacional de Astrofísica, Óptica y Electrónica (INAOE), Departamento de Electrónica, Apartado Postal 51 y 216, CP 72000, Puebla, México

**wwhm@inaoep.mx*

Abstract: We report the study of hydrogenated amorphous silicon-germanium (a-$Si_{1-X}Ge_X$:H) films prepared by low-frequency plasma-enhanced chemical vapor deposition (LF-PECVD) varying the composition ($0 \le X \le 1$). Silicon and germanium content is determined by energy dispersion spectroscopy (EDS). Refractive index, absorption coefficient and optical gap are estimated by transmittance measurements as well as by the use of PUMA software. Absorption coefficients obtained by using this software and by the Beer-Lambert law show good agreement according to absorption region. Results indicate that refractive index exhibits a linear behavior on germanium content for atomic percent (at.%). Employing these films and by the use of the finite-element software COMSOL, a single-mode low-contrast rib optical waveguide operating at the wavelength of 1550 nm is simulated, and later fabricated by using photolithography and plasma etching techniques. Measured optical losses are 7.6 dB/cm.

©2012 Optical Society of America

OCIS codes: (250.5300) Photonic integrated circuits; (230.7370) Waveguides; (310.6860) Thin films, optical properties; (160.6000) Semiconductor materials; (350.5400) Plasmas.

References and links

1. R. Soref, "The Past, Present, and Future of Silicon Photonics," IEEE J. Sel. Top. Quantum Electron. **12**(6), 1678–1687 (2006).
2. A. Scandurra, M. Lenzi, R. Guerra, F. G. Della Corte, and M. A. Nigro, "Optical Interconnects for Network on Chip," 1st International Conference on Nano-Networks and Workshops, Lausanne, September 2006.
3. J. A. Dionne, L. A. Sweatlock, M. T. Sheldon, A. P. Alivisatos, and H. A. Atwater, "Silicon-Based Plasmonics for On-Chip Photonics," IEEE J. Sel. Top. Quantum Electron. **16**(1), 295–306 (2010).
4. R. Soref, R. E. Peale, and W. Buchwald, "Longwave plasmonics on doped silicon and silicides," Opt. Express **16**(9), 6507–6514 (2008).
5. A. Vonsovici, G. T. Reed, and A. G. R. Evans, "β-SiC-on insulator waveguide structures for modulators and sensors systems," Mater. Sci. Semicond. Process. **3**(5-6), 367–374 (2000).
6. A. Sabac, C. Gorecki, M. Jozwik, L. Nieradko, C. Meunier, and K. Gut, "Technology and performances of silicon oxynitride waveguides for optomechanical sensors fabricated by plasma-enhanced chemical vapor deposition," J. Eur. Opt. Soc. **2**, 07026 (2007).
7. R. A. Soref, S. J. Emelett, and W. R. Buchwald, "Silicon waveguided components for the long-wave infrared region," J. Opt. A, Pure Appl. Opt. **8**(10), 840–848 (2006).
8. G. P. Agrawal, *Fiber-Optic Communication Systems* (Wiley, 2010).
9. M. Lipson, "Switching light on a silicon chip," Opt. Mater. **27**(5), 731–739 (2005).
10. G. T. Reed and A. P. Knights, *Silicon Photonics: An Introduction* (Wiley, 2004), Chap. 4.
11. L. Liao, D. Samara-Rubio, M. Morse, A. Liu, D. Hodge, D. Rubin, U. D. Keil, and T. Franck, "High speed silicon Mach-Zehnder modulator," Opt. Express **13**(8), 3129–3135 (2005).
12. G. Cocorullo, F. G. Corte, I. Rendina, C. Minarini, A. Rubino, and E. Terzini, "Amorphous silicon waveguides and light modulators for integrated photonics realized by low-temperature plasma-enhanced chemical-vapor deposition," Opt. Lett. **21**(24), 2002–2004 (1996).
13. A. Harke, M. Krause, and J. Mueller, "Low-loss singlemode amorphous silicon waveguides," Electron. Lett. **41**(25), 1377–1378 (2005).
14. G. Cocorullo, F. G. Della Corte, R. De Rosa, I. Rendina, A. Rubino, and E. Terzini, "Amorphous Silicon Waveguides and Interferometers for Low-Cost Silicon Optoelectronics," Proc. SPIE **3278**, 286–292 (1998).

#160438 - $15.00 USD Received 22 Dec 2011; revised 13 Feb 2012; accepted 28 Feb 2012; published 2 Mar 2012

15. R. Sun, J. Cheng, J. Michel, and L. Kimerling, “Transparent amorphous silicon channel waveguides and high-Q resonators using a damascene process,” Opt. Lett. **34**(15), 2378–2380 (2009).
16. A. Kosarev, A. Torres, C. Zúñiga, A. Abramov, P. Rosales, and A. Sibaja, “Effect of hydrogen dilution on electronic properties of a-SiH_x films deposited by low-frequency plasma,” J. Mater. Res. **18**(08), 1918–1925 (2003).
17. L. Pavesi and D. J. Lockwood, eds., *Silicon Photonics* (Springer-Verlag, 2004).
18. L. Liu, R. Kumar, K. Huybrechts, T. Spuesens, G. Roelkens, E.-J. Geluk, T. de Vries, P. Regreny, D. Van Thourhout, R. Baets, and G. Morthier, “An ultra-small, low-power, all-optical flip-flop memory on a silicon chip,” Nat. Photonics **4**(3), 182–187 (2010).
19. K. Ikeda, Y. Shen, and Y. Fainman, “Enhanced optical nonlinearity in amorphous silicon and its application to waveguide devices,” Opt. Express **15**(26), 17761–17771 (2007).
20. G. Y. Sung, N. M. Park, T. Y. Kim, K. H. Kim, K. S. Cho, and J. H. Shin, “High Efficiency Silicon Visible Light Emitter using Silicon Nanocrystals in Silicon Nitride Matrix and Transparent Doping Layer,” 2nd International Conference on Group IV Photonics, Belgium, September 2005.
21. M. Labrune, M. Moreno, and P. Roca i Cabarrocas, “Ultra-shallow junctions formed by quasi-epitaxial growth of boron and phosphorous-doped silicon films at 175°C by rf-PECVD,” Thin Solid Films **518**(9), 2528–2530 (2010).
22. Y. P. Chou and S. C. Lee, “Structural, optical, and electrical properties of hydrogenated amorphous silicon germanium alloys,” J. Appl. Phys. **83**(8), 4111–4123 (1998).
23. A. Kosarev, A. Torres, Y. Hernandez, R. Ambrosio, C. Zuniga, T. E. Felter, R. Asomoza, Y. Kudriavtsev, R. Silva-Gonzalez, E. Gomez-Barojas, A. Ilinski, and A. S. Abramov, “Silicon-germanium films deposited by low-frequency plasma-enhanced chemical vapor deposition: Effect of H_2 and Ar dilution,” J. Mater. Res. **21**(01), 88–104 (2006).
24. C. Iliescu and B. Chen, “Thick and low-stress PECVD amorphous silicon for MEMS applications,” J. Micromech. Microeng. **18**(1), 015024 (2008).
25. A. M. Pérez, C. Zúñiga, F. J. Renero, and A. Torres, “Optical properties of amorphous silicon germanium obtained by low-frequency plasma-enhanced chemical vapor deposition from SiH_4 + GeF_4 and from SiH_4 + GeH_4,” Opt. Eng. **44**(4), 043801 (2005).
26. L. Vegard, “Die Konstitution der Mischkristalle und die Raumfülung der Atome,” Z. Phys. **5**(1), 17–26 (1921).
27. K. Shimakawa, “On the compositional dependence of the optical gap in amorphous semiconducting alloys,” J. Non-Cryst. Solids **43**(2), 229–244 (1981).
28. M. E. Wieser, “Atomic weights of the elements 2005 (IUPAC Technical Report),” Pure Appl. Chem. **78**(11), 2051–2066 (2006).
29. R. Swanepoel, “Determination of the thickness and optical constants of amorphous silicon,” J. Phys. E **16**(12), 1214–1222 (1983).
30. http://en.wikipedia.org/wiki/Beer-Lambert_law.
31. E. G. Birgin, I. Chambouleyron, and J. M. Martínez, “Estimation of the Optical Constants and the Thickness of Thin Films Using Unconstrained Optimization,” J. Comput. Phys. **151**(2), 862–880 (1999), http://www.ime.usp.br/~egbirgin/puma/.
32. D. Poelman and P. F. Smet, “Methods for the determination of the optical constants of thin films from single transmission measurements: a critical review,” J. Phys. D Appl. Phys. **36**(15), 1850–1857 (2003).
33. G. Lifante, *Integrated Photonics: Fundamentals* (Wiley, 2003), Chap. 2.
34. J. Singh, *Optical Properties of Condensed Matter and Applications* (Wiley, 2006), Chap. 3.
35. K. Chew, S. F. Rusli, J. Yoon, Q. Ahn, V. Zhang, E. J. Ligatchev, T. Teo, T. Osipowicz, and F. Watt, “Gap state distribution in amorphous hydrogenated silicon carbide films deduced from photothermal deflection spectroscopy,” J. Appl. Phys. **91**(7), 4319–4325 (2002).
36. H. Kogelnik and V. Ramaswamy, “Scaling rules for thin-film optical waveguides,” Appl. Opt. **13**(8), 1857–1862 (1974).
37. R. A. Soref, J. Schmidtchen, and K. Petermann, “Large Single-Mode Rib Waveguides in GeSi-Si and Si on SiO_2,” IEEE J. Quantum Electron. **27**(8), 1971–1974 (1991).
38. S. P. Pogossian, L. Vescan, and A. Vonsovici, “The Single-Mode Condition for Semiconductor Rib Waveguides with Large Cross Section,” J. Lightwave Technol. **16**(10), 1851–1853 (1998).

1. Introduction

In recent years the microelectronics industry has been making efforts to overcome bottlenecks that silicon-based electronics has found. Some candidate approaches to overcome the bottlenecks, in addition to electron transport, include photon and plasmon transport, which individually or together could improve the technology that has been achieved to date [1–3]. In this regard, plasmo-opto-electronic integrated circuits (POEICs) proposed by Soref et al. [4] integrate all of them in a single chip. Optical waveguides are micro or nanometer structures that allow transmitting photons in the parallel direction of their axis in the visible and IR spectrum. These structures have different applications, e.g., sensing, photonic integrated circuits (PICs), optoelectronics [5–7], and one of the most important is in the field of telecommunications through optical fibers [8]. In this sense, silicon remains as a common

#160438 - $15.00 USD Received 22 Dec 2011; revised 13 Feb 2012; accepted 28 Feb 2012; published 2 Mar 2012
(C) 2012 OSA

element for their production, in the form of silica for optical fibers, and usually in crystalline (c-Si) structure for integrated optical waveguides along with SOI technology [9–11]. However, an attractive option for silicon-based integrated optical waveguides is the use of hydrogenated amorphous silicon (a-Si:H) [12,13] and its alloys with carbon or germanium, which exhibit low-absorption coefficient and low propagation losses in the second and third optical communications windows [14–16]. These materials can be obtained by plasma-enhanced chemical vapor deposition (PECVD) at low-temperatures (200-400 °C) enabling CMOS compatibility. Additionally to guided-wave functions, materials where light can be generated, processed and detected are required [2,17,18]. In this regard, PECVD semiconductors are promising candidates to perform the basic building blocks, i.e., generation, guiding, modulation and detection [19–21] of photons in the IR spectrum, on a monolithic c-Si wafer using the well-developed silicon technology.

Properties of materials deposited by PECVD depend strongly on the preparation parameters, such as: temperature, pressure, power of the source, frequency mode, feed and dilution gases, etc [21–24], having enough degrees of freedom to tailor their properties. From the design point of view, the control and tuning of their optical properties is a very attractive topic for optoelectronic device applications. For example, refractive index is one of them (it is 3.4 for c-Si and a-Si:H). In this sense, the incorporation of germanium aids to increase the refractive index of the hydrogenated amorphous silicon-germanium (a-$Si_{1-X}Ge_X$:H) alloy [25], which could act as the core of optical waveguides. This would potentially reduce the size of single-mode two-dimensional (2D) optical waveguides based on total internal reflection (TIR) confinement, by the refractive index increase [17].

In this manuscript, we investigate the optical properties of a-$Si_{1-X}Ge_X$:H films as a function of composition of germanium content in solid phase for silicon-based PICs applications. These properties will allow us to design an optical waveguide operating at 1550 nm, based on the TIR confining mechanism. Simulations have been carried to determine modal solutions using the finite-element method (FEM) commercial software COMSOL. In order to manufacture the proposed rib structure, deposition and etch rate parameters were characterized as a function of composition. Finally, by means of standard photolithography and plasma etching, single-mode structures were fabricated using a film that exhibits a value of 3.63 of refractive index. This film fills the requirements to obtain low-index contrast rib optical waveguides, a-$Si_{0.70}Ge_{0.30}$:H upon c-Si (Δn = 0.16). Propagation losses for this optical waveguide were determined by cut-back technique obtaining a value of 7.6 dB/cm.

2. Compositional properties of alloys

In 1921 Vegard [26] proposed Eq. (1) for calculations of crystal lattice, α, in alloys as a function of the concentration of the constituent elements, where A and B are composite elements in an A_XB_{1-X} alloy, and X is the atomic fraction of element A.

$$a_{AB}(X) = Xa_A + (1-X)a_B \tag{1}$$

Later, in 1981 Shimakawa [27] reported a study of the compositional dependence of the optical gap, E_g, of amorphous semiconducting alloys. Equation (2) describes the linear dependence between optical gap and composition for volume fraction, Y, of element A.

$$E_{AB}(Y) = YE_A + (1-Y)E_B \tag{2}$$

We have found that the refractive index in a-$Si_{1-X}Ge_X$:H alloys follows Vegard's law, i.e., a linear dependence between refractive index, n, and germanium content in solid phase, X (the atomic fraction), for a particular wavelength. This relation is described by Eq. (3):

$$n_{SiGe}(X) = Xn_{Ge} + (1-X)n_{Si} \tag{3}$$

#160438 - $15.00 USD Received 22 Dec 2011; revised 13 Feb 2012; accepted 28 Feb 2012; published 2 Mar 2012
(C) 2012 OSA

3. Experiment

a-$Si_{1-X}Ge_X$:H films were prepared by low-frequency plasma-enhanced chemical vapor deposition (LF-PECVD) in a planar reactor Reinberg model AMP3300. Glow discharge was maintained for 60 minutes at a frequency of 110 kHz, with a substrate temperature of 300 °C, pressure of 0.6 Torr and power of 600 W. Corning 2947 glass and n-type ρ = 1-5 Ω-cm <100> c-Si wafers were used as substrates. Silane (SiH_4) undiluted, and germane (GeH_4) diluted at 10% in hydrogen (H_2) were the feed gases, and H_2 the dilution gas. Germanium content in the gas phase is defined as $X_{Ge} = Q_{GeH4} / (Q_{GeH4} + Q_{SiH4})$, where Q_{GeH4} and Q_{SiH4} are the gas flows of germane and silane, respectively [22,23]. Four processes were realized varying the flow of GeH_4, $0 \leq X_{Ge} \leq 1$. Table 1 summarizes the gas flows in standard cubic centimeters per minute (sccm) of SiH_4, GeH_4 and H_2, showing also X_{Ge} and the thickness of the films, t, measured by means of a Veeco Dektak 150 stylus profilometer.

Table 1. Gas Flows for Deposition and Thickness of the a-$Si_{1-X}Ge_X$:H Films

Sample	X_{Ge}	Q_{SiH4} (sccm)	Q_{GeH4} (sccm)	Q_{H2} (sccm)	Thickness t (nm)
847	1.00	0	500	1000	1048
848	0.83	100	500	1000	981
849	0.60	100	150	1000	871
850	0	100	0	1000	680

Composition of the films was determined by energy dispersion spectroscopy (EDS) in the range 0-5 keV with a scanning electron microscope (SEM) model JEOL-JSM6610LV equipped with an EDS module. Our analysis ensures that the EDS signal comes only from the deposited films, because the energy is not enough to penetrate into the substrate. Optical properties were estimated by transmittance measurements by the use of a Perkin-Elmer lambda-3B spectrophotometer in the UV-Vis region (200-900 nm). Previous measurements were complemented in the near infra-red (NIR) region (900-4000 nm), by Fourier transform infra-red (FTIR) transmittance spectroscopy using a BRUKER spectrometer model Vector-22.

4. Results and discussion

4.1 Composition

Table 2 shows the composition of germanium and silicon in solid phase of the a-$Si_{1-X}Ge_X$:H films deposited on c-Si wafers, measured by EDS, which are listed by weight percent (w.%) and atomic percent (at.%).

Table 2. Germanium and Silicon Content of the a-$Si_{1-X}Ge_X$:H Films from EDS Measurements

		X (Ge)		X (Si)	
Sample	X_{Ge}	w.%	at.%	w.%	at.%
847	1.00	98.60	96.47	1.40	3.53
848	0.83	87.68	73.36	12.32	26.64
849	0.60	52.53	29.98	47.47	70.02
850	0	0	0	100	100

A small concentration of silicon was measured for sample 847, which could be attributed to remaining silicon left in the chamber from previous depositions. Figure 1 shows the results of EDS measurements, where the peaks localized at 1.18 keV and 1.74 keV correspond to germanium and silicon, respectively. The EDS module displayed data for atomic and weight percent. However, depending on characterization technique only one of them could be obtained. Conversion between weight and atomic percentage or vice versa can be made using

#160438 - $15.00 USD Received 22 Dec 2011; revised 13 Feb 2012; accepted 28 Feb 2012; published 2 Mar 2012
(C) 2012 OSA

the atomic weight (A_r) of element E, $A_r(E)$. Atomic weights for silicon and germanium are 28.0855 and 72.64 g/mol, respectively [28]. In order to convert germanium content in solid phase from weight fraction, X_w, to atomic fraction, X_{at}, we used Eq. (4):

$$X_{at} = \frac{X_w A_r(Si)}{X_w A_r(Si) + (1 - X_w) A_r(Ge)} \tag{4}$$

If the content of the elements is given in percentages, 100 must be used instead of 1. In order to convert from X_{at} to X_w, we used Eq. (5):

$$X_w = \frac{X_{at} A_r(Ge)}{X_{at} A_r(Ge) + (1 - X_{at}) A_r(Si)} \tag{5}$$

Shimakawa [27] proposed the use of atomic or molecular weights and densities for conversion purposes. Nevertheless, Eq. (4) and Eq. (5) fit better to the experimental data, as shown in Table 2.

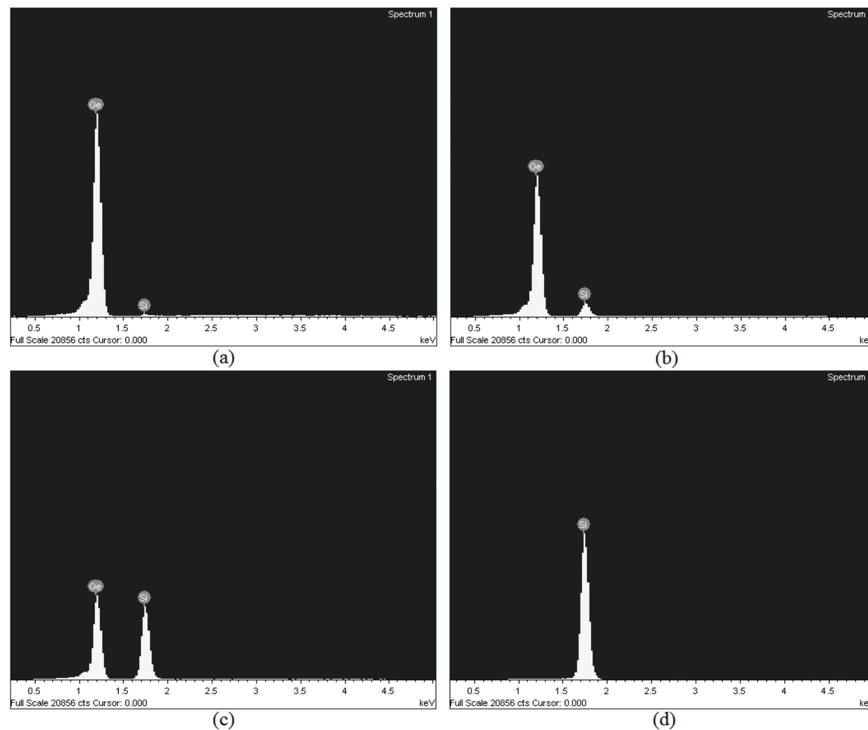

Fig. 1. EDS measurements of the samples 847-850, (a-d) respectively. Horizontal axis is in the range 0-5 keV; full-scale of vertical axis is 20856 cts.

4.2 Film growth

Deposition rate of the films increases as the germanium content in gas phase varies from 0 to 1. Figure 2(a) shows the nearly linear dependence of deposition rate on germanium content in solid phase for the weight fraction of the a-$Si_{1-X}Ge_X$:H films deposited on Corning 2947 glass substrates. Deposition rate was fitted using a linear Shimakawa-like function. In the plot also is shown the coefficient of determination (COD), R^2, obtained from the fit. Figure 2(b) shows the dependence of germanium content in solid phase on germanium content in gas phase.

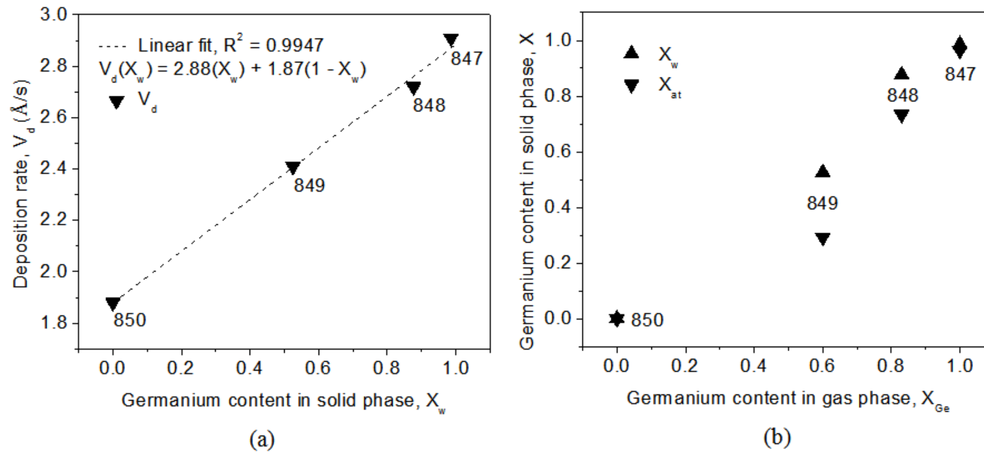

Fig. 2. (a) Deposition rate, V_d, as a function of germanium content in solid phase, X_w. (b) Germanium content on solid phase, X, as a function of germanium content on gas phase, X_{Ge}, of the a-$Si_{1-X}Ge_X$:H films.

4.3 Optical properties

Figure 3 shows conventional transmittance in the UV-Vis region (200-900 nm) and FTIR transmittance in the NIR region (900-4000 nm) of the a-$Si_{1-X}Ge_X$:H films deposited on Corning 2947 glass substrates. Interference fringes are correlated to optical properties, i.e., number of fringes is directly proportional to the thickness of the film, refractive index is proportional to the separation between the maxima and minima points of interference fringes [29], and finally, absorption coefficient is related to the enveloping shaped by the points at maximum of the interference fringes [25,29]. In conventional transmittance, the substrate Corning glass limits the maximum transmission to 91% in the transparent range (500-2500 nm). This is caused mainly by reflections at the air-glass and glass-air interfaces or some absorption due to the substrate. An advantage of FTIR transmittance is that it neglects substrate losses, so that it covers the entire range of transmission (0-100%). The optical gap of a-$Si_{1-X}Ge_X$:H films varies from 1.1 to 1.8 eV [23,25]. Therefore, the refractive index, absorption coefficient and the optical gap were estimated independently in the UV-Vis and NIR region (500-2500 nm) using transmittance measurements under two approaches: Beer-Lambert law [30] and pointwise unconstrained minimization approach (PUMA) software [31].

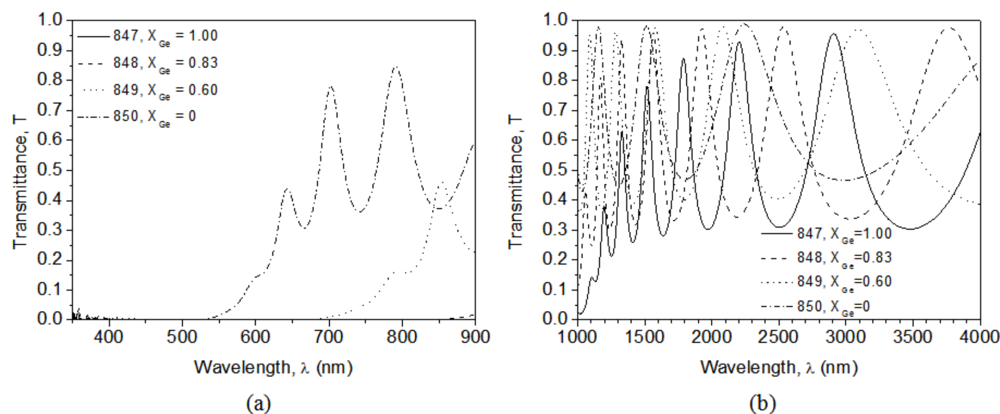

Fig. 3. (a) Conventional transmittance in the UV-Vis region, (b) FTIR transmittance in the NIR region of the a-$Si_{1-X}Ge_X$:H films.

#160438 - $15.00 USD Received 22 Dec 2011; revised 13 Feb 2012; accepted 28 Feb 2012; published 2 Mar 2012
(C) 2012 OSA

The Beer-Lambert law associates transmittance with absorbance and absorption coefficient through natural and common log functions, which are used for gases and liquids, respectively [30]. For solids the natural log is commonly employed over the entire spectral region [10]. Under this approach, measurements that neglect substrate effects are required, i.e., transmittance normalized to unity. Thus, the Beer-Lambert law can be applied properly to FTIR transmittance measurements in the NIR region, shown in Fig. 3(b), but not to conventional transmittance.

The Swanepoel method is highly reliable to estimate optical constants of thin films of amorphous semiconductor materials [29,32]. This method is implemented by PUMA software, which requires reflectance or transmittance measurements as an input file to estimate thickness and optical constants of refractive index and extinction coefficient of thin films [31]. PUMA software works with commercial substrates, i.e., transmittance must be referenced to some substrate. Hence, conventional transmittance measurements in the UV-Vis region, shown in Fig. 3(a), are appropriate to be used in PUMA software, but not for FTIR transmittance. Therefore, depending on the case, it is required to perform a normalization procedure: substrate normalization or unity normalization.

FTIR transmittance was normalized to the substrate using the dispersion relation of Corning 7059 glass: $s = (1 + (0.7568 - 7930\ \lambda^{-2})^{-1})^{1/2}$, where s is the refractive index of the Corning glass substrate, and λ is the wavelength of electromagnetic radiation given in nm [31]. On the other hand, the expression $T_s = 2s / (s^2 + 1)$ [29] relates the transmittance of the substrate, T_s, with its refractive index. Finally, FTIR transmittance is weighted by means of $T_{NS} = T_{FTIR}\ T_s$, where T_{FTIR} is FTIR transmittance and T_{NS} is the transmittance normalized to the substrate Corning 7059 glass. The transmittance of substrate Corning 7059 glass is also useful to perform normalization to unity of conventional transmittance, using $T_{NU} = T_C / T_s$, where T_{NU} is transmittance normalized to unity, and T_C is conventional transmittance.

Figure 4 shows the absorption coefficient in the UV-Vis region, where it can be observed that in the strong absorption region there is good agreement between the absorption coefficient obtained from the extinction coefficient, k, estimated with PUMA software using $\alpha = 4\pi k / \lambda$, and the absorption coefficient obtained from the Beer-Lambert law. This last coefficient was determined by applying the common log (Fig. 4(a)) and natural log (Fig. 4(b)) functions to conventional transmittance normalized to unity, T_{NU}, as well as the film thickness, t, as a multiplicative inverse factor. Nevertheless, the dependence for both approaches is not clear in the low-absorption region.

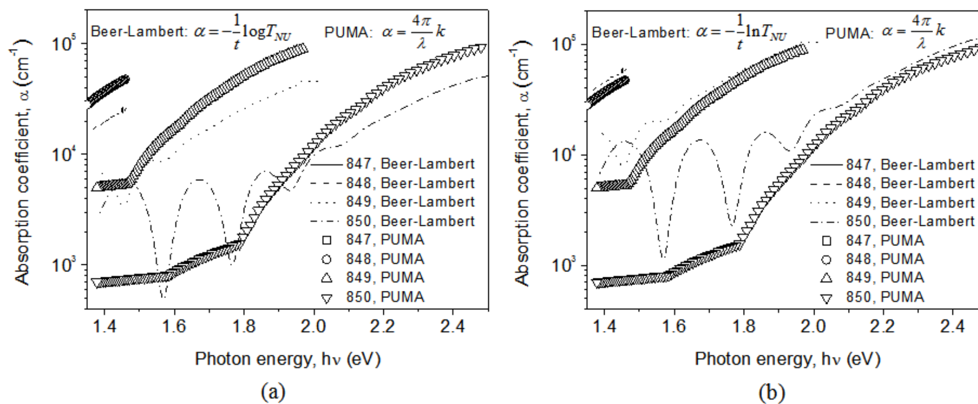

Fig. 4. Absorption coefficient from transmittance in the UV-Vis region, using the results of PUMA software and the Beer-Lambert law for (a) common and (b) natural log functions.

FTIR transmittance measurements allow observing more details in the low-absorption region. In Fig. 5 is observed that the film whose content is only germanium has a higher absorption coefficient than the films of silicon alloyed with germanium [22,23].

#160438 - $15.00 USD Received 22 Dec 2011; revised 13 Feb 2012; accepted 28 Feb 2012; published 2 Mar 2012
(C) 2012 OSA

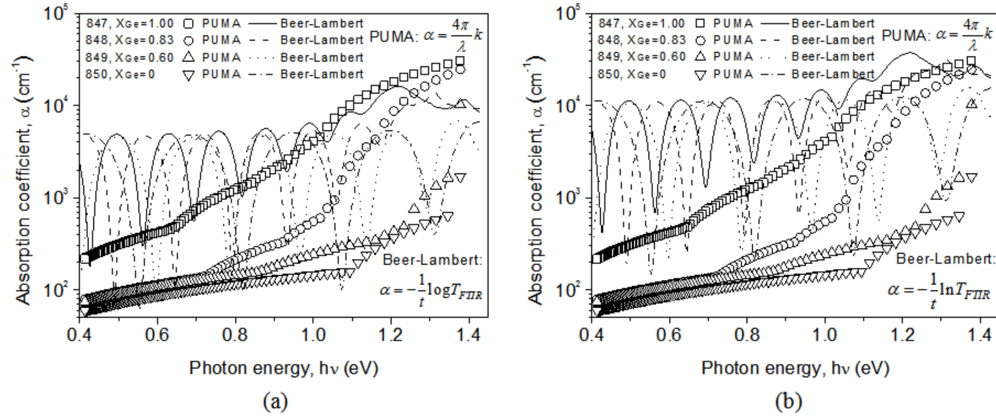

Fig. 5. Absorption coefficient from FTIR transmittance in the NIR region, using the results of PUMA and the Beer-Lambert law for (a) common log and (b) natural log functions.

The absorption coefficient obtained by PUMA software with the estimated extinction coefficient and previous normalization to substrate of FTIR transmittance, fits better with the common log than with the natural log function. In Fig. 5 it can be observed also that PUMA results act as an envelope for interference fringes obtained from the Beer-Lambert law applied to FTIR transmittance measurements. These results are important for theoretical determination of propagation losses in an optical waveguide. It is well known that there are several sources of losses [5,10]. However, considering only losses caused by absorption of the material, Eq. (6) relates propagation losses of a passive optical waveguide with its absorption coefficient.

$$\Gamma = \frac{1}{L} 10 \log(10^{-\alpha L}) = -10\alpha \tag{6}$$

Where Γ represents propagation losses in dB/cm, α is the absorption coefficient in cm^{-1}, and L is the length of the medium through which light is transmitted. However, the constant 10 in Eq. (6) differs with the previously reported of 4.343 based on exponential attenuation, $e^{-\alpha L}$, typically employed for SOI technology [10,33]. Nevertheless, Cocorullo et al. [14], reported experimental and theoretical propagation losses (Γ) of 0.7 dB/cm and 0.98 dB/cm, respectively, for an a-Si:H optical waveguide of α = 0.08 cm^{-1}. Substituting these last values (Γ and α) in Eq. (6), ratios of –0.7/0.08 = –8.75 and –0.98/0.08 = –12.25, are obtained. These values are more approximated to –10, as shown in Eq. (6), rather than –4.343. Difference between natural log and common log is a constant of 2.303 (i.e., ln 10 or 10/4.343) [30].

The spectral dependence of the absorption coefficient was used to characterize the optical gap of the a-$Si_{1-X}Ge_X$:H films by Tauc's method, using $(\alpha(h\nu)h\nu)^{1/2} = B^{1/2}(h\nu - E_g)$. The B parameter is defined as $B = (e^2 L(m_e^* m_h^*)^{3/2})/(nc\varepsilon_0 \hbar^3 (2m_e^*)^2)$, where m_e^* and m_h^* are the effective masses of electrons and holes, respectively, n is the refractive index, c is the speed of light, ε_0 is the permittivity of free space, e is the electron charge, L is the interatomic separation, and $\hbar$ is the reduced Planck constant [34]. Assuming that the optical gap is known, germanium content in the solid phase can be estimated for the volume or weight fraction using the Shimakawa relation. The results are listed in Table 3, and shown graphically in Fig. 6.

Table 3 shows the B parameter that was obtained from the fit by using the Tauc relation. This parameter is inversely proportional to germanium content and refractive index as can be observed in the previous expression for the B parameter. On the same table, it is observed also that germanium content in solid phase (obtained from Shimakawa relation using E_g^{04}), is very approximate to germanium content in solid phase for the weight percent, shown previously in Table 2. A COD up to 0.99 was obtained for all fits.

#160438 - $15.00 USD Received 22 Dec 2011; revised 13 Feb 2012; accepted 28 Feb 2012; published 2 Mar 2012
(C) 2012 OSA

Table 3. Optical Gap, Germanium Content and B Parameter of the a-$Si_{1-X}Ge_X$:H Films

Sample	X_{Ge}	PUMA E_g^{Tauc} (eV)	PUMA X_w	PUMA $B \times 10^5$ ($cm^{-1}eV^{-1}$)	Beer-Lambert law E_g^{Tauc} (eV)	Beer-Lambert law X_w	Beer-Lambert law $B \times 10^5$ ($cm^{-1}eV^{-1}$)	$\alpha = 10^4$ cm^{-1} (PUMA) E_g^{04} (eV)	$\alpha = 10^4$ cm^{-1} (PUMA) X_w
847	1.00	0.87	1.00	2.03	0.87	1.00	-	1.09	1.00
848	0.83	1.05	0.80	3.28	1.03	0.80	-	1.22	0.85
849	0.60	1.34	0.48	4.46	1.31	0.48	4.58	1.52	0.52
850	0	1.78	0	5.06	1.74	0	5.28	1.98	0

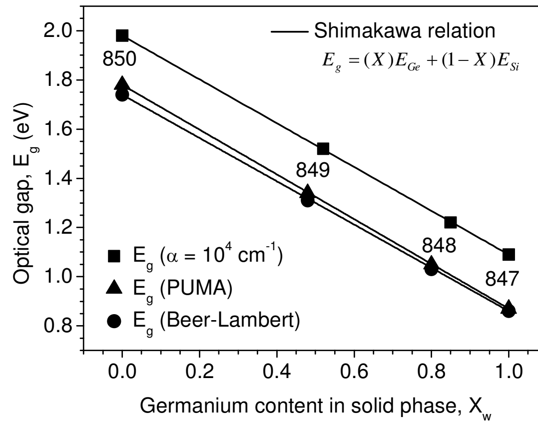

Fig. 6. Estimation of germanium content in solid phase from optical gap by the use of Shimakawa relation.

Figure 7 shows refractive index estimated by means of the PUMA software, including the values of refractive index at the three optical communication windows: 830, 1310 and 1550 nm of wavelength.

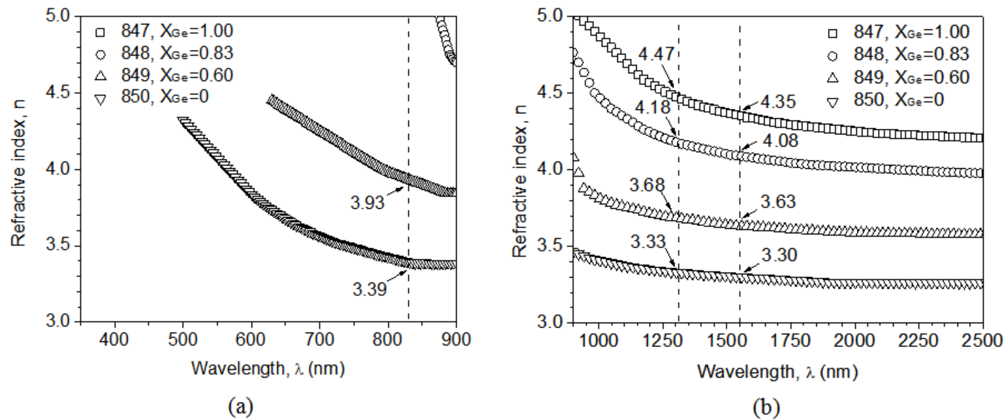

Fig. 7. Refractive index estimated by means of the PUMA software from (a) UV-Vis conventional transmittance, and (b) FTIR transmittance. Vertical dashed lines are located at 830, 1310 and 1550 nm of wavelength.

Plotting refractive index, shown in Fig. 7(b), as a function of germanium content in solid phase for X_w and X_{at}, listed in Table 2, we obtained the plot shown in Fig. 8, which displays a

#160438 - $15.00 USD Received 22 Dec 2011; revised 13 Feb 2012; accepted 28 Feb 2012; published 2 Mar 2012
(C) 2012 OSA

linear dependence between refractive index and germanium content in solid phase for the atomic fraction. These data were fitted using Eq. (3).

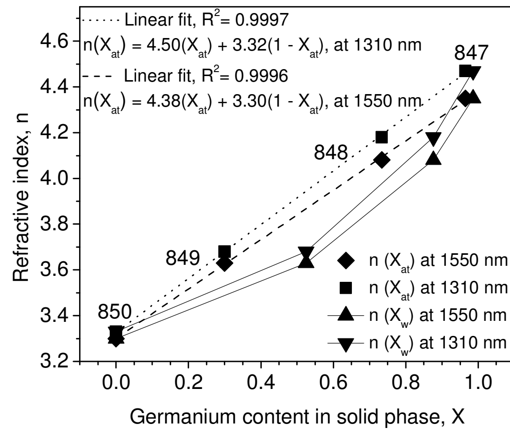

Fig. 8. Refractive index as a function of germanium content in solid phase of the a-$Si_{1-X}Ge_X$:H films.

Refractive index for sample 847, obtained from the fit, is slightly higher than that estimated by PUMA software, because this film contains a small amount of silicon (see Table 2). The theoretical refractive index for an a-Ge:H film would be 4.5 at 1310 nm, and 4.38 at 1550 nm, as can be seen in Fig. 8.

Among several models and definitions for optical gap, E_g at 10^3 and 10^4 cm^{-1}; difference of mobility edges of conduction and valence bands, $E_g = E_c - E_v$; Tauc's method, E_g^{Tauc}, etc [34,35], Eq. (3) represents a highly reliable alternative for characterization and design purposes, providing information about refractive index and compositional properties of amorphous semiconducting alloys.

5. PIC: optical waveguides

5.1 Design

Optical waveguides can be designed using the theory for 1D and 2D optical waveguides: normalized dispersion relations [36] and Soref's formula: $a/b \leq c + r/(1 - r^2)^{1/2}$, where $c = 0.3$, r is the thickness ratio, a and b are the width and height of the optical waveguide, respectively [37]. Correction for $c = -0.05$ was made by Pogossian et al. [38]. Often, the solutions of the propagating modes of an optical waveguide are required. These were solved numerically by the FEM software package COMSOL Multiphysics along with the RF module, which is appropriate for mode analysis in the optical region. Figure 9 shows the results of simulations of the single-mode low-contrast rib optical waveguide.

#160438 - $15.00 USD Received 22 Dec 2011; revised 13 Feb 2012; accepted 28 Feb 2012; published 2 Mar 2012
(C) 2012 OSA

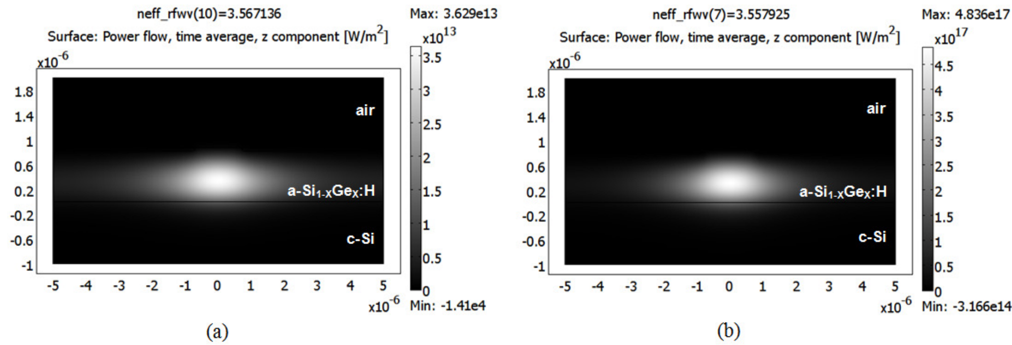

Fig. 9. Simulations of the single-mode low-contrast rib optical waveguide for (a) quasi-TE and (b) quasi-TM mode.

Figure 9(a) shows the effective refractive index for quasi-TE mode (3.5671), whereas Fig. 9(b) shows the effective refractive index for quasi-TM mode (3.5579). Characteristics used for simulation of the rib structure were as follows: refractive index of 3.63 for core (a-$Si_{0.70}Ge_{0.30}$:H film), 1 for upper cladding (air), and 3.47 for lower cladding (c-Si). Width of the core (a) was 1.5 µm, height of the core (b) was 0.87 µm, with a thickness ratio (r) of 0.94. According to Soref's formula, these parameters satisfied the single-mode condition for a low-contrast rib optical waveguide.

5.2 Fabrication and characterization

Rib optical waveguides were fabricated via standard photolithography and plasma etching. Positive photoresist ma-P 1225 was used for photolithography, removing it with acetone after masking. Control of rib height is a critical step; for this reason etch rate was characterized using several samples, whose germanium content in the solid phase varies, using a reactive ion etching (RIE) system in capacitive mode at RF (13.56 MHz) and room temperature. SF_6/O_2 and CF_4/O_2 were the gas mixtures for plasma etching, with a flow ratio of 50/10 sccm and pressure of 40 mTorr. A power of 50 W was used for SF_6/O_2, maintaining glow discharge during 80 seconds with a measured self-bias voltage of 71 V. For the CF_4/O_2 mixture a power of 150 W was used, maintaining glow discharge during 50 seconds with a measured self-bias voltage of 332 V.

Figure 10(a) shows the results of vertical etch rate, V_V, using the conditions previously described, and the profile of some structures obtained with the SF_6/O_2 mixture (Fig. 10(b)), and CF_4/O_2 mixture (Fig. 10(c)). These structures were of good enough uniformity and high degree of anisotropy, observing good definition of waveguide patterns and a good adherence between film and photoresist. Etch rate for the SF_6/O_2 gas mixture, exhibited a linear dependence on germanium content in solid phase for the weight fraction. On the other hand, CF_4/O_2 gases mixture revealed a nonlinear behavior.

#160438 - $15.00 USD Received 22 Dec 2011; revised 13 Feb 2012; accepted 28 Feb 2012; published 2 Mar 2012
(C) 2012 OSA

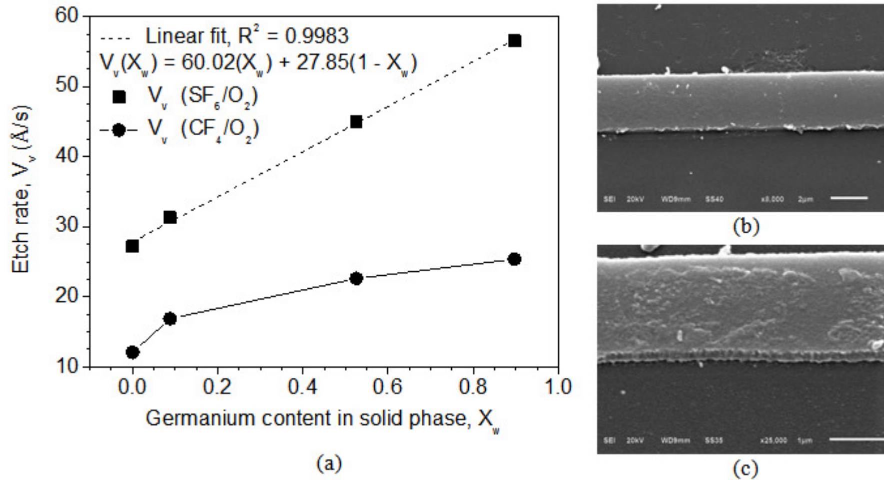

Fig. 10. (a) Etch rate as a function of germanium content in solid phase, X_w, for SF_6/O_2 and CF_4/O_2 gases mixtures. (b) Structure of 3 μm of width from SF_6/O_2. (c) Structure of 1.5 μm of width from CF_4/O_2.

The designed optical waveguide was fabricated using sample 849 (a-$Si_{0.70}Ge_{0.30}$:H film) deposited on a C-Si wafer, and employing the conditions for the SF_6/O_2 gas mixture. Propagation losses for the resulting optical waveguide, were measured by means of the cut-back technique using a linear polarized coherent laser beam operating at a wavelength of 1550 nm. Figure 11(a) shows propagation losses that were determined from the slope of the linear fit. Figure 11(b) corresponds to optical waveguides of 1.5 μm of width (optical image), whereas Fig. 11(c) corresponds to an optical waveguide of 15 μm of width (SEM image).

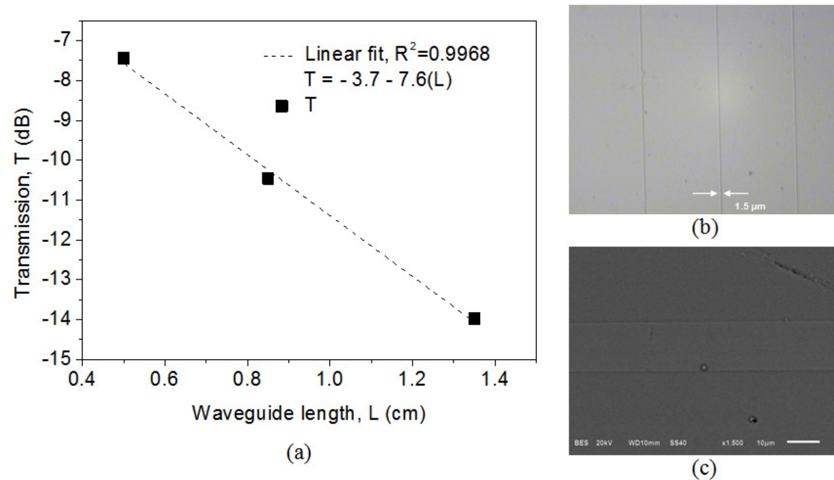

Fig. 11. (a) Propagation losses obtained from the low-contrast single-mode rib optical waveguide by cut-back technique. (b) Optical waveguides of 1.5 μm of width. (c) Optical waveguide of 15 μm of width.

Comparing the propagation losses obtained from the cut-back technique with the absorption spectra, shown in Fig. 5(a), a significant difference was observed because the absorption coefficient measured by transmittance is not suitable for the low-absorption region. Additional techniques for subgap absorption are required, such as: photothermal deflection spectroscopy (PDS) [35] or constant photocurrent method (CPM) [16].

#160438 - $15.00 USD Received 22 Dec 2011; revised 13 Feb 2012; accepted 28 Feb 2012; published 2 Mar 2012
(C) 2012 OSA

6. Conclusions

We have obtained optical and compositional properties of hydrogenated amorphous silicon-germanium alloys. We have found linear dependences for refractive index, deposition and etch rate parameters. In particular, the refractive index showed a linear dependence on germanium content in solid phase for the atomic fraction. Optical gap, deposition rate and etch rate with the SF_6/O_2 gas mixture, were nearly linear as a function of germanium content in solid phase for the weight fraction. Expressions have been proposed for this binary alloy to convert from atomic to weight fraction and vice versa. Properties of alloys typically exhibit linear behavior as a function of the constituent elements, however, the key point is the determination of whether atomic or weight fraction corresponds to a given property. We have also observed a dependence on absorption region: the Beer-Lambert law with the common log function shows good agreement with the data estimated by PUMA software in the low-absorption region, and as was expected, the Beer-Lambert law with natural log function shows good agreement with the data estimated by PUMA software in the strong absorption region. This fact yields a relation between propagation losses and absorption coefficient for amorphous semiconducting alloys. The proposed low-contrast single-mode rib optical waveguide could be suitable for low confining applications. However, some issues concerning optimization of the material for integrated photonics applications have to be addressed. As a future work, the deposition and etching of the films must be realized in a careful way in order to reduce the surface roughness and by consequence reduce radiation losses.

Acknowledgments

The authors gratefully acknowledge José Soto and Enrique Sánchez from IFUAP-BUAP, México, for providing support with profilometry measurements; Margarita Galindo and Carla de la Cerna from BUAP, México, for assistance with EDS/SEM measurements; and technical staff of Microelectronics Laboratory and LNN from INAOE for preparation of samples. This work was supported by CONACYT under research project 51241-Y and student scholarship 224193.

#160438 - $15.00 USD Received 22 Dec 2011; revised 13 Feb 2012; accepted 28 Feb 2012; published 2 Mar 2012
(C) 2012 OSA

200.23.5.162 {ts '2018-10-26 17:23:12'}